AR REVIEWS IN ADVANCE10.1146/annurev.matsci.36.111904.135144
(Some corrections may occur before final publication online and in print)

Annu. Rev. Mater. Res. 2006. 36:49–79
doi: 10.1146/annurev.matsci.36.111904.135144

First published online as a Review in Advance on January 24, 2006

POSITRON ANNIHILATION AS A METHOD TO CHARACTERIZE POROUS MATERIALS

David W. Gidley, Hua-Gen Peng, and Richard S. Vallery
Department of Physics, University of Michigan, Ann Arbor, Michigan 48109-1040; email: gidley@umich.edu, pengh@umich.edu, vallery@umich.edu

Key Words porous films, pore size, low dielectric constant, positronium

■ **Abstract** Beam-based positron annihilation spectroscopy (PAS) is a powerful porosimetry technique with broad applicability in the characterization of nanoporous thin films, especially insulators. Pore sizes and distributions in the 0.3–30 nm range are nondestructively determined with only the implantation of low-energy positrons from a table-top beam. Depth-profiling with PAS has proven to be an ideal way to measure the interconnection length of pores, search for depth-dependent inhomogeneities or damage in the pore structure, and explore porosity hidden beneath dense layers or diffusion barriers. The capability of PAS is rapidly maturing as new intense positron beams around the globe spawn more accessible PAS facilities. After a short primer on the physics of positrons in insulators, the various probe techniques of PAS are briefly summarized, followed by a more detailed discussion of the wide range of nanoporous film parameters that PAS can characterize.

INTRODUCTION

The concept of using antimatter to probe matter should not seem surprising given the rich variety of particles aimed at characterizing materials properties: electrons, neutrons, muons, protons, and helium nuclei, for example, as well as photons of virtually every wavelength from microwaves to visible light to X rays to gamma rays. The simplest and most readily used antimatter probe is the positron (the antiparticle to the electron). When a positron is injected into materials, it will eventually annihilate with an electron with the complete conversion of the pair's combined mass, m, into high-energy photons with total energy E, given by Einstein's famous formula $E = mc^2$. The premise in using positrons to probe materials is that understanding the physics of matter-antimatter annihilation allows one to then extract nanoscale materials information specific to the location at which the annihilation takes place. The physical state from which this annihilation occurs generally can be divided into free positron annihilation (with electrons in the target material) or positronium (Ps) annihilation (Ps is the hydrogen-like bound state of a positron with an electron captured from the material). The critical motivation for characterizing porous materials is that both positrons and positronium tend to

18 Jan 2006 10:5 AR ANRV279-MR36-02.tex XMLPublish[SM](2004/02/24) P1: IKH
AR REVIEWS IN ADVANCE10.1146/annurev.matsci.36.111904.135144

seek out and localize in vacancies/voids in metals and insulators. Simple coulomb attraction forces positrons into electron-decorated vacancies in metals, whereas in insulators the reduced dielectric interaction in a void energetically favors trapping neutral Ps in low-density regions.

For this review of positron annihilation spectroscopy (PAS) in porous materials, our primary focus is on materials that form the Ps bound state by electron capture when positrons are injected into them (hence the "P" in PAS is interchangeably used for Ps or positron). Moreover, we restrict our view of porous materials to a subset of "nanoporous" materials (see Reference 1 for a nice review), which are generally considered to have ordered or disordered porosity in the pore size range of 1–1000 nm. For practical reasons we focus on 1–50 nm pores in typically disordered/amorphous systems that could be organic or inorganic. We note that PAS has been used for 30–40 years to sensitively detect monovacancies and small vacancy clusters in metals and semiconductors (2), whereas Ps annihilation spectroscopy has been developed over a similar period to probe subnanometer, intermolecular voids in polymers (3). The extension of Ps annihilation spectroscopy into materials with engineered nanoporosity is a natural outgrowth of the recent surge in interest in nanotechnology coupled with advances in positron beam technology that allow controlled implantation of positrons into technologically important thin films, especially low-k dielectric films in the microelectronics industry (4–6).

A number of spectroscopies have been developed to parameterize the annihilation process—generically called positron annihilation spectroscopy (PAS) even though the positron may be annihilating from the Ps state. The three main spectroscopies are in the time domain (how long the positron lives before annihilation), the energy of the annihilation gamma rays, and the momentum of the gamma rays (Doppler energy shifts and angular distribution of the gamma rays). A brief overview of these spectroscopies is given below to provide some breadth of the field. In addition, because these PAS were initially developed using radioactive beta-decay positron emitters that embed positrons deeply ($\sim$0.1 mm) into materials, the thin films encountered in modern nanotechnology demand low-energy beams to control the positron implantation depth. For detailed discussions on depth-profiled PAS, the reader is referred to Schultz & Lynn's (2) comprehensive review on beam-based PAS methodologies in metal and semiconductor films and at interfaces. We focus here on beam-based positron/Ps annihilation spectroscopy because its precise positron implantation control is often essential for characterizing nanoporous systems.

After a brief introduction to the physics of positrons and Ps in porous insulators, we present an overview of the various annihilation spectroscopies commonly in use. The remainder of the review focuses on those parameters of interest to the nanoporous materials researcher that PAS can help to characterize. Foremost among these are the pore size, pore size distribution (PSD), and pore interconnection length (L_{int}, the scale length over which pores are connected to each other). The difficulties of absolute porosity determination with PAS are considered along with compensating capabilities of porosity calibration, relative porosity determination,

18 Jan 2006 10:5 AR ANRV279-MR36-02.tex XMLPublish[SM](2004/02/24) P1: IKH
AR REVIEWS IN ADVANCE10.1146/annurev.matsci.36.111904.135144

and sensitivity to processing-induced changes. A unique strength associated with beam-based PAS is the capabilities to depth-profile by controlling the positron implantation energy and to resolve laterally by finely focusing the beam on a small spot on the target. The capability to nondestructively detect depth-dependent pore structural characteristics even when the pores are buried under barrier layers will be an increasingly attractive capability as nanoporous films and composites become more complex.

PS IN NANOPOROUS FILMS

The most important aspect of applying PAS to nanoporous insulators begins with the natural formation of Ps when positrons are injected into a material. The generation and subsequent behavior of Ps in porous films, through the use of a beam of positrons, are depicted in Figure 1. When a positron (50 eV to 15 keV) is implanted into thin films, the positron will scatter off atoms and electrons in the solid and slow to atomic-scale energy (several eV) within picoseconds. Typically 10–50% of these positrons can either capture a bound molecular electron [the Ore model of Ps formation (7)] or slow even more and recombine with free "spur" electrons liberated by the positron's ionizing collisions [the spur model (8)] to form the bound state of Ps. [It is interesting to note that a detailed relationship between

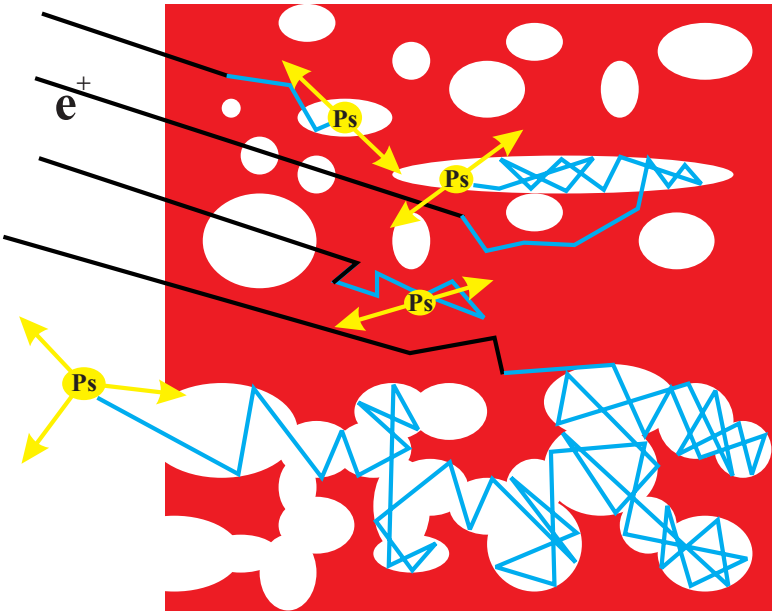

Figure 1 Positronium formation in porous materials.

18 Jan 2006 10:5 AR ANRV279-MR36-02.tex XMLPublish[SM](2004/02/24) P1: IKH
AR REVIEWS IN ADVANCE10.1146/annurev.matsci.36.111904.135144

the physics of these two Ps formation mechanisms and the chemical and material properties of the film, and hence their relative contributions to Ps formation, are largely unknown (9, 10).] Ps has two states, singlet (*para*-) and triplet (*ortho*-), depending on the relative spin state (0 for *para* and 1 for *ortho*) of the positron and electron. The self-annihilation lifetime of *para*-Ps (*p*-Ps) is short, 125 ps, and this rapid singlet annihilation occurs with the emission of two back-to-back gamma rays of 511 keV (2γ annihilation conserving momentum and energy). However, *ortho*-Ps (*o*-Ps) in vacuum is required to annihilate into at least three photons (3γ annihilation) in order to conserve angular momentum, and this slower, triplet process has a long, characteristic lifetime of 142 ns (11). Lifetime spectroscopy can easily distinguish this long-lived triplet state of Ps. Moreover, unlike the 2γ decays that are clustered in a narrow peak at 511 keV, the distribution in gamma-ray energy of any one annihilation photon from 3γ triplet-Ps decay is reasonably approximated by a linear increase from zero energy to a maximum cutoff at 511 keV. Hence gamma-ray energy spectroscopy can also easily distinguish these different decay modes. Triplet Ps plays the key role in probing porous materials, as its annihilation can be strongly perturbed by singlet interactions with surrounding electrons that measurably reduce the *o*-Ps lifetime and the $3\gamma/2\gamma$ branching ratio while it is localized in the pores.

In insulating materials, Ps will preferentially locate in electron-deficient defects, such as vacancies, cracks, pores, and voids of all kinds. The reduced dielectric response of the medium in a void leads to a higher binding energy for Ps, and thus Ps near a void is pushed into it. Once inside the potential well of the void, Ps will eventually trap there after it loses a small amount of energy, as depicted in Figure 1. The singlet interaction of the positron in the *o*-Ps with surrounding molecularly bound electrons of opposite spin shortens the lifetime of the Ps by mixing in the fast 2γ decay mode during wall collisions. The process wherein the positron in the Ps annihilates not with its bound electron but with a surrounding electron of opposite spin is called "pickoff" annihilation, a 2γ process that can decrease the Ps lifetime from 142 ns to as low as 1 ns. More comprehensive reviews of positron-material interactions can be found elsewhere (7, 12).

The behavior of Ps from formation to annihilation can be analyzed by PAS to provide a variety of information about the structural properties of the material. An overview of the more detailed discussions in the following sections is presented here. Pore size is the most straightforward property to deduce. Over several decades, the lifetime of Ps (Ps is hereafter assumed to be *ortho*, triplet positronium unless specifically designated to be in the *para*, singlet state) has been correlated to the size of packing voids in polymeric materials. The correlation for micropores ($R \leq 2$ nm) is very successful with the use of the time-honored quantum mechanical Tao-Eldrup model (13, 14). On the other hand, the extension of this model for mesopores ($R > 2$ nm) has been implemented only in the past decade (15, 16). This success has a significant impact on the analysis of engineered nanoporous materials, which tend to include mesopores. If the pores are closed (like swiss cheese, as in the upper part of Figure 1), then Ps should be trapped in a pore. In classical terms, the Ps bounces around in the pores like a gas atom, and smaller

18 Jan 2006 10:5 AR ANRV279-MR36-02.tex XMLPublish[SM](2004/02/24) P1: IKH
AR REVIEWS IN ADVANCE10.1146/annurev.matsci.36.111904.135144

pores will cause more/faster pickoff annihilation, i.e., a shorter Ps lifetime and enhanced 2γ annihilation, and vice versa. Furthermore, a distribution of Ps lifetimes occurs if there is a PSD. Techniques have been developed for deducing a PSD from continuum lifetime fitting of the annihilation lifetime distribution and are discussed below.

An important feature in the characterization of porous structure has to do with the length scale over which pores may be connected to each other. Ps is light and mobile and may diffuse within a porous network over long distances that can be greater than even the porous film thickness, as depicted in the schematic structure in the lower half of Figure 1 (we estimate that Ps can make approximately 10^6 pore wall collisions before annihilation). Ps escaping into vacuum annihilates completely by 3γ annihilation with the vacuum lifetime of 142 ns, telltale indicators that the pores in the film are interconnected. In the case of fully interconnected (i.e., percolated) pores, all the Ps attracted into the mesopores diffuses out of the film. However, more typically, only part of the Ps residing in the mesopores escapes out of the film. This is because the engineered pores can be quite tortuous, and some part of the pores may be closed to the partially interconnected porous network. Using a simple Ps diffusion model, we have been able to deduce an average pore interconnection length from profiling the film by implanting positrons into various depths. If the pores are highly interconnected, then to extract the average pore size (technically, the mean-free path for Ps in the interconnected pores), it is necessary to deposit a thin diffusion barrier on top of the film to keep the Ps corralled in the porous network. PAS techniques can then monitor the annihilation of Ps in the network of the porous film. The average measure of pore size in such a network (effectively one very large pore extending throughout the film) is the mean-free path $= 4\,V/S$, where V and S are the pore volume and pore surface area, respectively. Specifics are discussed below.

PAS TECHNIQUES

There are several complementary spectroscopic methods in use to characterize porous materials using PAS. In all these techniques, the gamma rays from the annihilation of either the positron or positronium are detected. The techniques differ primarily in the manner of detecting the gamma ray and in the subsequent analysis of the spectrum. The techniques are Doppler-broadening spectroscopy (DBS), angular correlation of annihilation radiation (ACAR), Ps time-of-flight (Ps-TOF), 3γ annihilation spectroscopy (3γ branching ratio, or $3\gamma/2\gamma$), and positron(ium) annihilation lifetime spectroscopy (PALS). We present here a brief overview (see also Reference 6) of each of these techniques, but complete reviews of PAS methodology and other positron techniques that have been used extensively to probe a wide range of media can be found elsewhere (2, 7, 17, 18).

Although the implantation of positrons from radioactive β^+ decay sources directly into the sample of interest (bulk-PAS) is a straightforward technique with which to study materials, this approach is unsuitable for thin films, given the high

18 Jan 2006 10:5 AR ANRV279-MR36-02.tex XMLPublish^{SM}(2004/02/24) P1: IKH
AR REVIEWS IN ADVANCE10.1146/annurev.matsci.36.111904.135144

energies and broad energy range of the positrons from the source. The implementation of positron beams (17) overcomes this obstacle by delivering focused, monoenergetic positrons onto the sample. Broadly speaking, a positron beam takes the high-energy positrons from β^+ decay or pair-production and, via moderation (2), cools them to eV energies, accelerates and transports them to a target, and focuses them onto the sample at a defined energy. Besides enabling the study of thin films, positron beams also offer the important capability of depth-profiling the sample by varying the implantation energy of the incident positrons. All the PAS techniques discussed herein make extensive use of the capabilities of positron beams. One minor disadvantage of using a beam is that the sample is located in the vacuum system required for the beam.

Positrons for a beam are derived a number of ways (17), including from radioactive sources or from pair-production in either a linear accelerator or a nuclear reactor. These energetic positrons are then moderated through the use of semicrystalline metal foils or cryogenic noble gases. The low-energy positron beam is then transported electrostatically or magnetically. Beams based on a radioactive source are compact lab-scale devices that can deliver $<10^7$ positrons sec^{-1} and as such have the capacity to be deployed in an industrial environment. Facility-scale beams using pair-production from linacs and nuclear reactors have the potential for higher positron rates approaching 10^{10} positrons sec^{-1}.

DBS and ACAR are designed to be sensitive to the momentum of the electron-positron pair at the moment of annihilation. This momentum is largely determined by the momentum of the electron in free positron annihilation or by the relative formation fraction of Ps and hence can probe the electronic and physical environment in which positrons are implanted. DBS uses high-energy-resolution gamma detector(s), typically high-purity germanium detector(s), to acquire an energy spectrum of 2γ annihilation events in a window centered around 511 keV. These 2γ events correspond to free positron annihilation, *p*-Ps annihilation, or Ps pickoff quenching events, and in the rest frame of the annihilation, this produces two gamma rays of precisely 511 keV each. In the laboratory frame, however, the measured energy of annihilation may be Doppler shifted owing to the center-of-mass motion of the annihilating pair, hence leading to a Doppler-broadened, and in some cases Doppler-shifted, annihilation peak. DBS derives a large amplification in sensitivity whereby the pair momentum corresponding to only a few eV of kinetic energy produces keV energy shifts for gamma rays emitted along the pair momentum owing to the unique process of annihilation of massive particles into massless photons. In practice one defines two parameters that quantify the annihilation: They are obtained by first identifying a narrow energy window centered on 511 keV (annihilation at rest). The S-parameter is the ratio of events in this window to all 511 keV events, which emphasizes the relative fraction of low-momentum events, whereas the W-parameter is the ratio of integrated events in a "wing" region to the total peak and is a relative measure of high-momentum annihilations.

The S- and W-parameters can yield interesting information regarding the voids in the film. Generally speaking, annihilation in voids should have less

18 Jan 2006 10:5 AR ANRV279-MR36-02.tex XMLPublish[SM](2004/02/24) P1: IKH
AR REVIEWS IN ADVANCE10.1146/annurev.matsci.36.111904.135144

high-momentum core electron annihilation and/or more Ps formation, both leading to a higher S-parameter. The S-parameter can also be sensitive to the chemistry of the film and increases in environments in which Ps quenching is large, for example, in films in which paramagnetic centers have been introduced (6) or in which there are free radicals present. However, whereas DBS can explore relative changes of the S- and W-parameters as a function of film porosity, without sufficient calibration DBS has difficulty in determining the relative contributions of all the effects that can influence the pair momentum. The pore size cannot be determined. Two variations of DBS involve using two germanium detectors simultaneously (coincidence-DBS) (19) or measuring the S-parameter as a function of annihilation time [age-momentum correlation (AMOC)] (20). The coincidence-DBS technique offers significantly better energy resolution, is capable of distinguishing chemical environments, and may be useful in probing the pore surface chemistry.

The ACAR technique also measures the momentum of the electron-positron pair upon annihilation, but rather than measuring the energy broadening of the 511 keV gamma rays, it measures the relative angle between them (and hence the component of pair momentum transverse to the gamma ray direction). At rest, positrons, *p*-Ps, or Ps quenching annihilates into two back-to-back (180°) gamma rays. If the annihilating pair is moving relative to the lab frame, then the gamma rays will deviate from 180° by a small angle θ (typically 10 mrad); the angle is larger for higher-momentum annihilations. A typical ACAR experimental setup has two position-sensitive detectors (Anger cameras), which are placed approximately 5 meters apart (18) and which have an angular resolution on the order of milliradians. The location of time-coincident 511 keV gamma rays is detected, and the deviation angle is calculated. This two-dimensional ACAR technique has many of the same sensitivities and limitations as the DBS technique. ACAR is positron rate intensive and generally requires an intense positron beam facility to achieve acceptable analysis times for a beam-based depth-profiling system.

Ps-TOF spectroscopy of Ps emission has recently been applied to porous media with highly interconnected pores (11, 21, 22). A TOF spectrometer utilizes a positron beam to form Ps near the surface of a film with an interconnected network of pores. A narrow collimated gamma shield is placed in front of at least one detector (typically plastic scintillator) a short distance away from the front of the sample. Ps that escapes the film into vacuum travels into the collimator window and may annihilate; the time of the annihilation is recorded. This time histogram can then be converted into an energy distribution for Ps that escapes the film. If the energy of the positron beam is varied, the degree to which the Ps in the film can thermalize, and hence its energy upon its escape, can be varied. This is most useful in understanding Ps thermalization and diffusion in the pores and thus in determining whether the pores are interconnected (22). Information on pore sizes is not determined directly through Ps-TOF measurements, and more importantly, the technique is not applicable if the pores in the film are closed.

Although the techniques discussed above are useful in characterizing certain aspects of material porosity, the most widely used positron annihilation

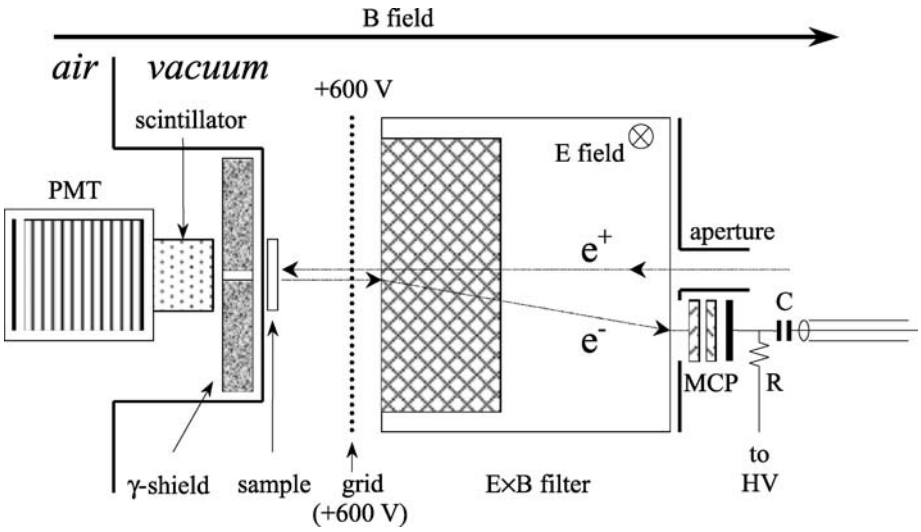

Figure 2 The magnetically guided PAS beam/spectrometer at Washington State University. From Reference 4.

spectroscopies are positron/positronium annihilation lifetime spectroscopy (PALS) (23–25) and $3\gamma/2\gamma$ positron annihilation spectroscopy (26–29). These complementary techniques offer the widest range of information on the pore morphology in the film, and both make extensive use of positron beams to determine pore size and pore interconnectivity while searching for depth-dependent film inhomogeneities (details are discussed in the next section).

The $3\gamma/2\gamma$ technique acquires an energy spectrum of positron and Ps annihilation in the film. Figure 2 shows a typical setup. Positrons are implanted into the material and will either annihilate directly or form Ps that will annihilate via several possible channels, as described above (see Ps in Nanoporous Films). Annihilation into two photons (2γ) produces a peak at 511 keV and Compton scattered events distributed from zero up to the Compton cutoff at 341 keV. Annihilation into three photons (free *o*-Ps annihilation) produces a uniformly increasing energy distribution from 0—511 keV for any individual photon. The total energy spectrum of annihilation photons is a combination of the 2γ and 3γ spectra. To identify the 2γ part of the spectrum, which corresponds to direct positron and parapositronium annihilation or Ps quenching on the pore wall, the events are integrated for an energy window set around the photopeak region of 511 keV. The remainder of the spectrum at lower energy, which includes free Ps annihilation and Compton scattered photopeak events, is integrated. The $3\gamma/2\gamma$ ratio is then calculated, after correction for the Compton events, by normalizing to a spectrum that contains only positron 2γ annihilation (28, 30). Through the varying of film temperature and/or porosity, trends in the $3\gamma/2\gamma$ ratio are investigated, and

18 Jan 2006 10:5 AR ANRV279-MR36-02.tex XMLPublish[SM](2004/02/24) P1: IKH
AR REVIEWS IN ADVANCE10.1146/annurev.matsci.36.111904.135144

information on the pore structure is deduced. In films with larger pores or higher porosity, the number of events that self-annihilate in the 3γ part of the spectrum increases.

Rather than investigating the energy/momentum domain of Ps annihilation, as the other PAS techniques do, PALS is done in the time domain. Positrons are implanted into the material, and the time between the implantation and the detection of any annihilation gamma ray is measured. Through the use of PALS with thin films, a magnetically guided (Figure 2) or an electrostatically focused (Figure 3) positron beam of several keV is transported and focused on a target in a high-vacuum system. The beam is usually generated using a sealed, commercially available, ^{22}Na radioactive beta-decay positron source (Figure 3), but other positron generation schemes are available [e.g., pair-production by high-energy photons (31)]. Methods for detecting the implantation of the positron (start signal) vary depending on the type of positron beam. The systems shown in Figure 2 and Figure 3 use a channel electron multiplier array to detect a secondary electron emitted when the positron strikes the target surface. Beams based on trapping and accumulating positrons in electromagnetic wells trigger the start signal synchronously with the ejection of the positron from the trap (17). The subsequent detection in a fast-timing gamma detector of any one of the annihilation gamma rays provides the stop signal, and the time difference between start and stop is determined with standard fast-timing electronics.

A PALS spectrum is a lifetime histogram of all the annihilation events of the implanted positrons. It is a combination of several exponentially decaying lifetime components and may involve a continuum of lifetime components as well. Figure 4 presents examples of typical lifetime spectra. Every beam-PALS spectrum contains at least two lifetime components: One is less than 0.5 ns and involves the prompt annihilation of positrons that do not form Ps (the peak marking $t = 0$ in Figure 4), and the other is the vacuum positronium lifetime of 142 ns. The pore-sensing Ps lifetime components, typically one to three, are related to the voids of various sizes that may exist in the material. Spectrum fitting programs, such as POSFIT (32) or LT (33), are used to deconvolve the system's fast time resolution and determine the primary fitted data: the Ps lifetimes and their corresponding relative intensities. Additionally, the time spectrum can be fit to a continuum of lifetimes (34, 35) to extract a distribution of pore sizes (36). However, the uniqueness of this method of fitting is a well-known problem. Further discussion of the fitting and interpretation of the lifetime spectrum is below. The great advantage of this timing technique is that the individual states from which the positron annihilates are delineated through their lifetime because *p*-Ps, free positrons, and *o*-Ps each have distinct time signatures. Indeed, triplet Ps annihilation may have several signature lifetimes corresponding to annihilation in micropores, mesopores, or vacuum. Differentiation by lifetime and relative intensity of each process is tremendously valuable in the interpretation of the spectrum as the key step in the process of deducing a fully consistent view of the porous microstructure.

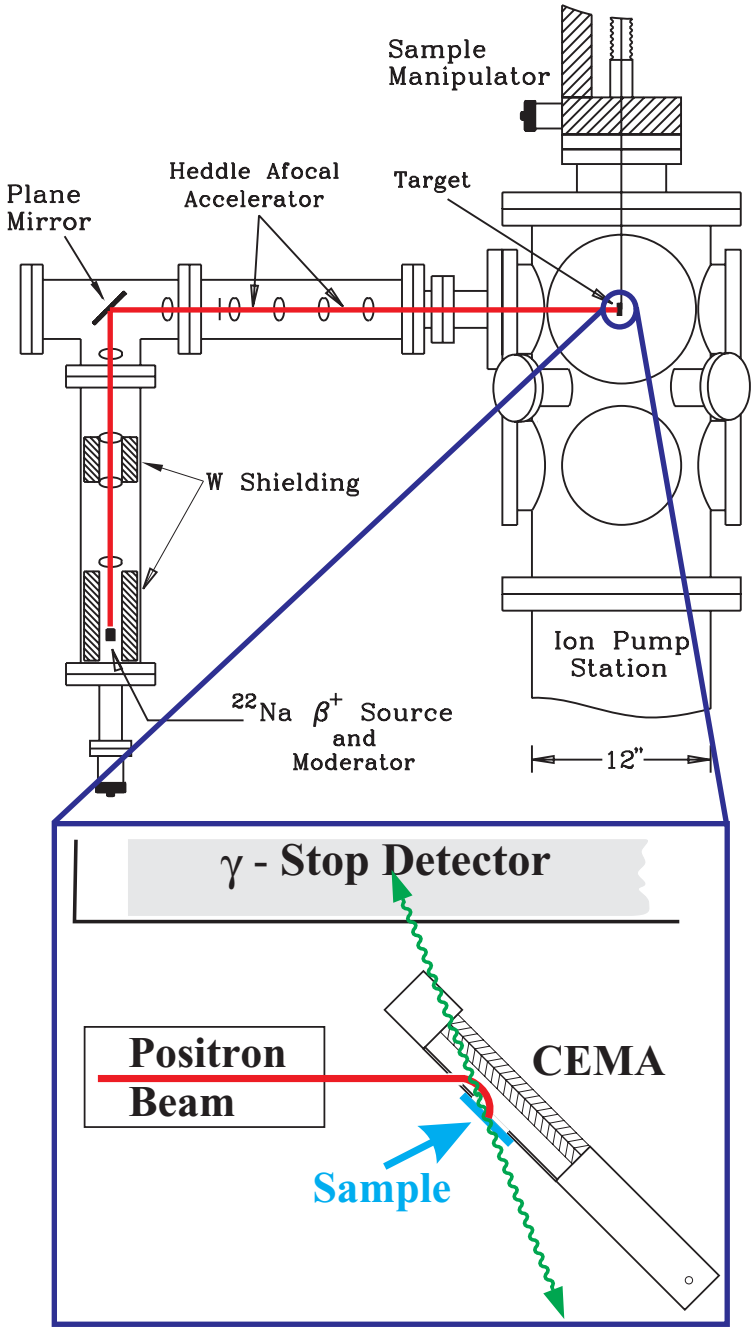

Figure 3 Schematic of the Michigan depth-profiled PALS spectrometer. From Reference 4.

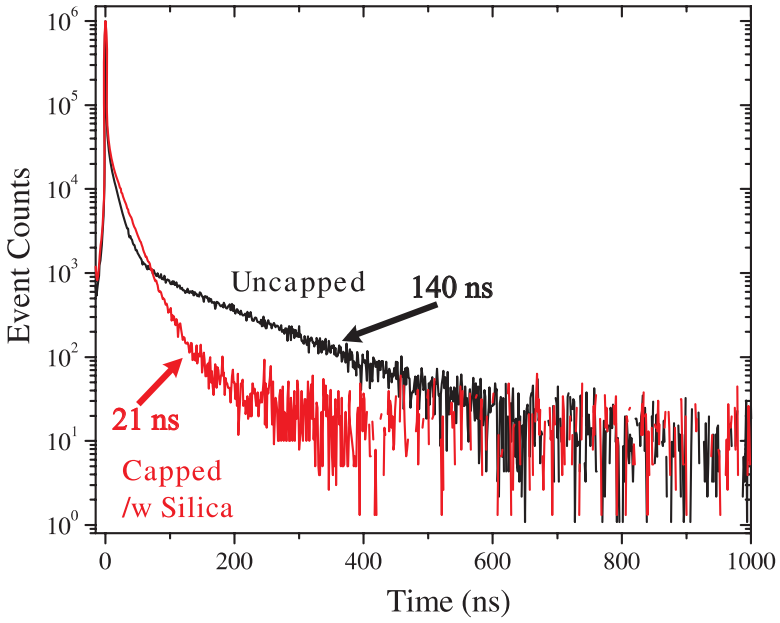

Figure 4 Typical Ps lifetime spectra for a film with open porous network (*black*) and after capping (*red*).

PORE CHARACTERIZATION WITH PAS

The key feature in probing porous insulating materials with PAS is the ability to monitor the formation, diffusion, and annihilation of *o*-Ps, as depicted in Figure 1. The techniques that sense the positron-electron pair momentum at the instant of annihilation (ACAR and DBS) are not as sensitive to pore structure details as are the lifetime (PALS) and energy (3γ) spectroscopies, which are directly sensitive to the formation and complete history of the long-lived, 3γ decay of *o*-Ps. Most of our discussion of pore characterization centers on these two spectroscopies. Our presentation, however, reveals our philosophical preference for PALS, which details and differentiates the time evolution of each individual component of *p*-Ps, free positrons, and *o*-Ps in micropores, mesopores, or vacuum. The $3\gamma/2\gamma$ ratio is one number representing a time integral over all these undifferentiated components and requires deconvolution. It certainly complements PALS and can offer some additional advantage in terms of simplicity and count rate (5).

Determination of Pore Size

PALS and $3\gamma/2\gamma$ spectroscopy each have the attractive feature of a direct one-to-one connection between fitted Ps lifetime:$3\gamma/2\gamma$ branching ratio and pore size

18 Jan 2006 10:5 AR ANRV279-MR36-02.tex XMLPublish[SM](2004/02/24) P1: IKH
AR REVIEWS IN ADVANCE10.1146/annurev.matsci.36.111904.135144

for that Ps trapped in the pores. The quantum mechanical model that Tao (14) and Eldrup (13) first developed in the early 1980s has been empirically used to calibrate Ps lifetimes of several nanoseconds with the sizes of micropores, such as those in polymers of ~0.6 nm in diameter (37). In this simple model, Ps is localized in an infinitely deep potential well and undergoes pickoff annihilation with molecular electrons only when it is within a short distance of the pore surface. Consistent with the model's assumptions, one can then calculate the pickoff annihilation rate, λ_{pickoff}, for a given size and shape pore. The total Ps decay rate, λ, and Ps lifetime, τ, are related as

$$\lambda = 1/\tau = \lambda_{\text{pickoff}} + \lambda_{\text{vac}},$$

where λ_{vac} is just 1/(142 ns). With only the ground state of Ps in the well populated in the Tao-Eldrup model, the model is insufficient for characterizing larger mesopores when the pore diameter approaches the thermal De Broglie wavelength of Ps (approximately 6 nm). Thermally excited states of Ps atoms in the pore must also be included in the calculation (16).

The Tao-Eldrup model has been extended to characterize voids throughout the nanopore range. To summarize the results (15, 16, 25), it is assumed that the Ps atoms randomly sample all the states in a rectangular well with a probability governed by the Maxwell-Boltzman distribution (thermalized Ps in the well is assumed). At a given temperature and assumed pore shape, a curve measuring lifetime versus pore dimension can then be calculated. It is useful to convert such curves from a pore shape–specific dimension to a classical mean-free path, $l = 4\,V/S$, where V/S is the pore's ratio of volume to surface area (15). As the mean distance between Ps pore wall collisions, the mean-free path is a linear measure of pore size that is not specific to any particular pore geometry. Figure 5 shows the pickoff-shortened curves measuring Ps lifetime versus mean-free path at several different temperatures. The model includes only one universal fitting parameter that is determined by existing experimental data for l below 2 nm. For insulators this parameter is assumed to be material independent, although in principle, some degree of material specificity would be expected. In the past 5 years the Michigan positron group has participated in many round-robins in which a variety of film samples have been shared by different groups to compare pore sizes measured with different techniques. PALS agrees quite well overall with other methods (Figure 5, right panel). PALS tends to measure pore diameters that are slightly larger than those measured with SANS, slightly smaller than those measured with EP, and in excellent agreement with those measured with BET. The pore size calibration appears to be very reliable, but the issue of material specificity needs further research.

Using the calculated Ps lifetime within the pore, one can easily determine the $3\gamma/2\gamma$ branching ratio because the lifetime-shortening effect of pore wall pickoff is solely a 2γ annihilation process. Hence, the branching ratio is theoretically simply $\lambda_{\text{vac}}/\lambda_{\text{pickoff}}$ for that particular fraction of Ps annihilating in the pores. Because Ps in the pores is not as cleanly delineated as it is by its lifetime in PALS and because

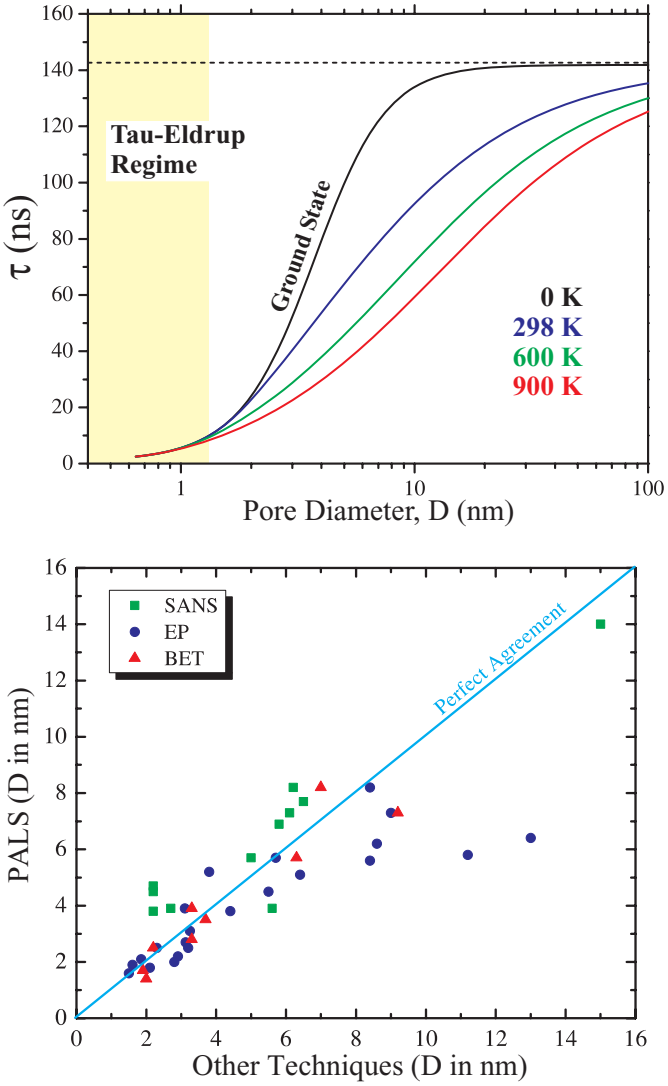

Figure 5 (*Top*) Pore size calibration calculated at different temperatures versus mean-free path. (*Bottom*) Recent round-robin comparisons of PALS pore diameters with those measured by small-angle neutron scattering (SANS), ellipso-metric porosimetry (EP), and gas absorption (BET).

the measured branching ratio is convolved with detector efficiencies and Compton scattering effects, the connection between $3\gamma/2\gamma$ ratio and pore size is not as direct as for PALS.

Pore Size Distribution

There are two primary methods for fitting lifetime spectra to characterize porosity in the material. POSFIT (32) and LT (33) are commonly used to fit the spectra to a prompt time-resolution function convolved with multiple discrete lifetimes and corresponding intensities. Typical porous films require two to six discrete lifetimes to account for the range of micropore to mesopores in the material, which are then straightforwardly converted into pore size (or mean-free path), as described above. The primary advantage of discrete lifetime fitting is that it is a relatively robust procedure that determines the average size of the pores in the material. However, this analysis can be complicated by multiple-lifetime spectra that occur when micropores and mesopores coexist, and each may involve a distribution of pore sizes.

To further characterize the porosity of a film, pore size distributions (PSDs) are determined by fitting the decay spectrum to a continuum of lifetimes, through the use of either CONTIN (35) or MELT (34), which are then converted into fractional pore volume as a function of spherical (or cylindrical) pore diameter. The peaks of the resulting distributions typically are in good agreement with the average pore sizes determined from discrete fitting. Figure 6 shows PSD results acquired at several positron beam energies for a rather exotic dielectric film in which the pore structure is changing rapidly with depth below the surface. One limitation of PSD fitting is the uniqueness of the fitting results (a common problem in continuum fitting). Thus, the continuum fits are typically referred to as plausible PSDs. When interconnected pores are involved, the concept of PSD in PALS starts to lose meaning. In a percolated film each Ps atom samples the entire network and hence has the same mean-free path; a single Ps lifetime (not a distribution) results.

Determination of Film Porosity

In the section above, we showed how direct the physical interpretation of the fitted Ps lifetime, and to a slightly lesser extent the complementary measurement of $3\gamma/2\gamma$ branching ratio, are in regard to pore size. The interpretation of the fitted relative intensity in each Ps lifetime component in the lifetime spectrum in terms of film porosity is not as straightforward (see, e.g., Reference 38). Whereas the pore size calibration with lifetime is quite universal in insulators, there are a number of factors, beyond porosity, that influence the relative intensity of Ps annihilating in the pores. The inherent Ps formation fraction depends on the material chemistry of the insulator and can be significantly altered by additives and free radicals. Moreover, pore size affects the relative intensity of Ps annihilating in the pores even for films of identical porosity and chemistry—thus, the absolute porosity calibration must depend in a more complicated way on both Ps intensity and pore

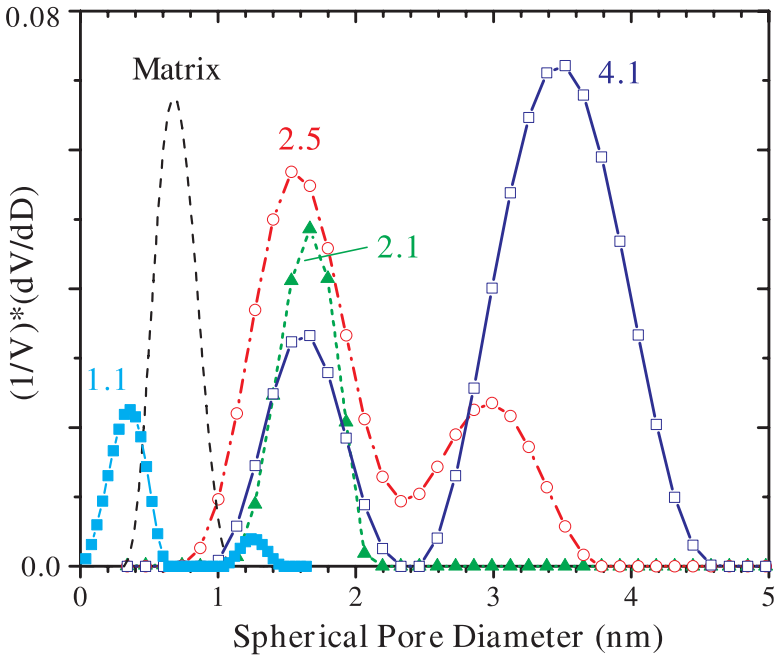

Figure 6 Plausible PSDs in a low-k film for a variety of positron beam energies (in keV) determined from continuum lifetime fitting. This film has a complicated depth dependence to porosity. The curve labeled "matrix" has no engineered pores.

size, not intensity alone. This interdependence on pore size can be seen in Figure 7, which shows three films with distinctly different pore generators (porogens) in a common methyl-silsesquioxane (MSSQ) matrix. The plotted intensity includes the sum of Ps annihilating in the mesopores and Ps that diffuses through the interconnected mesopores to escape into vacuum. Hence, $I_{Ps,Film}$ is a total measure of how much Ps finds its way into mesopores and should be related to the porogen-induced mesoporosity. In these films there is a clear monotonic trend upward in $I_{Ps,Film}$ with increasing mesoporosity (left graph), and the rate of rise correlates well with the measured pore size (right graph). At any given porosity the host matrix "wall" thickness between large pores is greater than that for small pores. For Ps to populate the mesopores, it must be formed in the matrix and diffuse/hop through the matrix's micropores. As porosity rises and/or pore size decreases, the wall thickness between pores shrinks, which favors the diffusion of Ps into the mesopores. As a result, $I_{Ps,Film}$ increases at the expense of the Ps intensity annihilating in the micropores (total Ps formation is almost constant, increasing by less than 10% over the full porosity range). As observed, saturation of the mesopore Ps intensity occurs at lower porosity for smaller pores. Without knowing the film porosity from a complementary technique (as in Figure 7), we would be

18 Jan 2006 10:5 AR ANRV279-MR36-02.tex XMLPublish[SM](2004/02/24) P1: IKH
AR REVIEWS IN ADVANCE10.1146/annurev.matsci.36.111904.135144

hard-pressed to deduce absolute porosity simply from fitted Ps intensity or $3\gamma/2\gamma$ ratio, as there is no unique correspondence of these parameters to porosity.

Despite the more complicated dependence of fitted Ps intensity on porosity, pore size, and film chemistry, the curves in Figure 7 do indeed represent the absolute calibration of porogen-induced mesoporosity. This calibration relies on an independent measure of porosity and hence is not fundamentally a stand-alone PAS measure, but this limitation may be quite acceptable in a production environment in which the matrix-porogen system can be well calibrated. On their own, PALS fitting of Ps intensity and lifetime (pore size) and $3\gamma/2\gamma$ branching ratio are more effective in determining relative porosity in porous films with unchanged chemistry. With extensive study to determine the mobility of Ps in the micropores of the matrix walls between pores (the Ps diffusion or hopping length) and the mechanism of Ps formation in this material (9, 10), it is possible to independently interpret the physical significance of the fitted Ps intensities from first principles and material structure.

Depth-Profiling of Films

METHODOLOGY A particularly powerful feature of beam-based PAS is the ability to control the mean depth at which positrons are implanted into the film by simply adjusting the energy with which the incoming positrons strike the target. The implantation profile can be determined with the use of a well-tested transmission model (2, 39, 40) and is shown in Figure 8 for a positron beam incident at $\sim 45^\circ$ with the target surface. The mean positron implantation depth, $\bar{Z}$, is given for normal incidence of the beam by $\bar{Z} = (40/\rho)\, E^{1.6}$, where E is the positron beam energy in keV and ρ is the film density in g cm^{-3}. The implantation profile is roughly bell-shaped and ranges from the surface of the film to approximately twice the mean depth. Therefore, the best depth resolution occurs for low energy (shallow implantation). This positron implantation profile corresponds quite closely to the Ps formation depth-profile (there may be several nm spreading owing to the electron-positron correlation process to form Ps), but this does not necessarily correspond to the Ps annihilation profile. If the pores are interconnected, then the Ps may diffuse a long distance away from its formation location. Hence, the fitted Ps lifetime may reflect an average over a large region of the film sampled by each Ps atom, but even so the Ps formation intensity is still characteristic of the location of formation. Depth-dependent variations in this Ps intensity (and the distribution of Ps) among the different Ps lifetime components) may reflect changes in porosity with depth. Of course, if the pores are isolated and trap Ps, then the lifetime will also indicate any pore size variation with mean implantation depth, as we illustrate below. Such depth-profiling of depth-dependent pore morphology is straightforward, but profiling a perfectly homogeneous film can also reveal a fundamental pore shape parameter: the pore interconnection length. This parameter, which is particularly unique to PAS analysis, is discussed below (see Pore Interconnection Length).

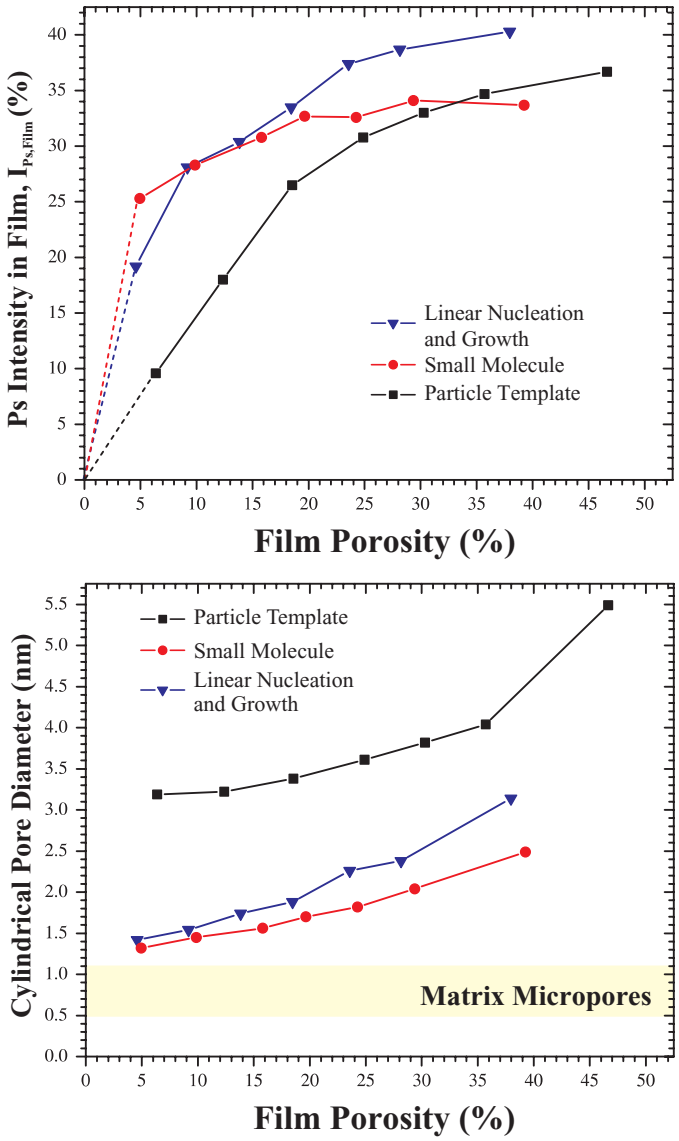

Figure 7 Plots of Ps intensity annihilating in the film (*top*) and measured pore diameter versus porosity (determined using refractive index and the Lorentz-Lorenz equation) (*bottom*) for films made with three different porogens. Together the intensity and diameter can be used as a measure of relative porosity in chemically similar films. Films supplied by R.D. Miller of IBM, Almaden Research Center.

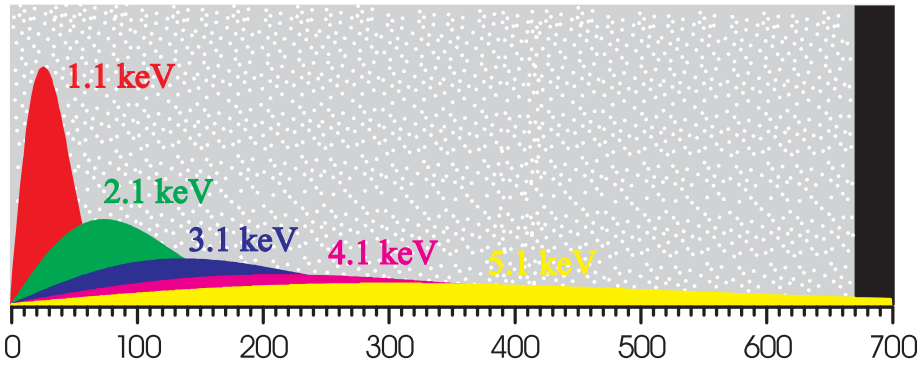

Figure 8 Positron implantation profiles for several beam energies calculated for ∼45° incidence on a film of density 1 g cm^{-3}.

PORE INTERCONNECTION LENGTH By depth-profiling a porous material, one can measure the length over which the nanopores, especially those that are engineered or porogen-induced, are interconnected. Pore interconnection is a measure of pore clustering prior to percolation of the film and as such can depend sensitively on film porosity (percolation occurs when a pore extends through the film). Ps is light, small, and able to withstand a million collisions with the pore walls (25). If the pores are fully interconnected, Ps can thus diffuse through 1000 nm–thick porous films, escape from the film, and annihilate in vacuum with the telltale signatures of a long 142 ns lifetime and high $3\gamma/2\gamma$ ratio. Partially interconnected pores at lower film porosity will result in a much smaller measured Ps diffusion length that is determined by the pore interconnectivity. By straightforwardly measuring the fraction of Ps that escapes from the film, F_{esc}, as a function of mean positron implantation depth, as shown in Figure 9, we were able to deduce the pore interconnection length, L_{int}, of the mesopores. By applying a diffusion model to Ps in the film, we were able to calculate L_{int} of the mesopores to be the mean implantation depth from which approximately 50% of Ps escapes from the film.

The nanoporous films analyzed in Figure 9 are MSSQ hosts with ∼1.50 nm pores generated by a degradable porogen. PAS depth-profiling, a physically simple and direct interpretation of pore connection, determines the average depth over which porogen-induced nanopores are connected to the surface. As evident in the left plot, deeper implantation results in lower Ps escape as more Ps traps and annihilates in pores that are not connected to the surface. Once Ps is in these mesopores, it is energetically trapped from returning to the micropores of the MSSQ matrix (25, 41), and therefore Ps diffusion is governed solely by the nanopore morphology. As such, PAS may be the ideal probe for studying the fundamental formation process, structural characterization, and evolution with porosity of the strategically introduced nanopores without the interference of the matrix microporosity in the analysis. Moreover, as the porogen-induced porosity of the film

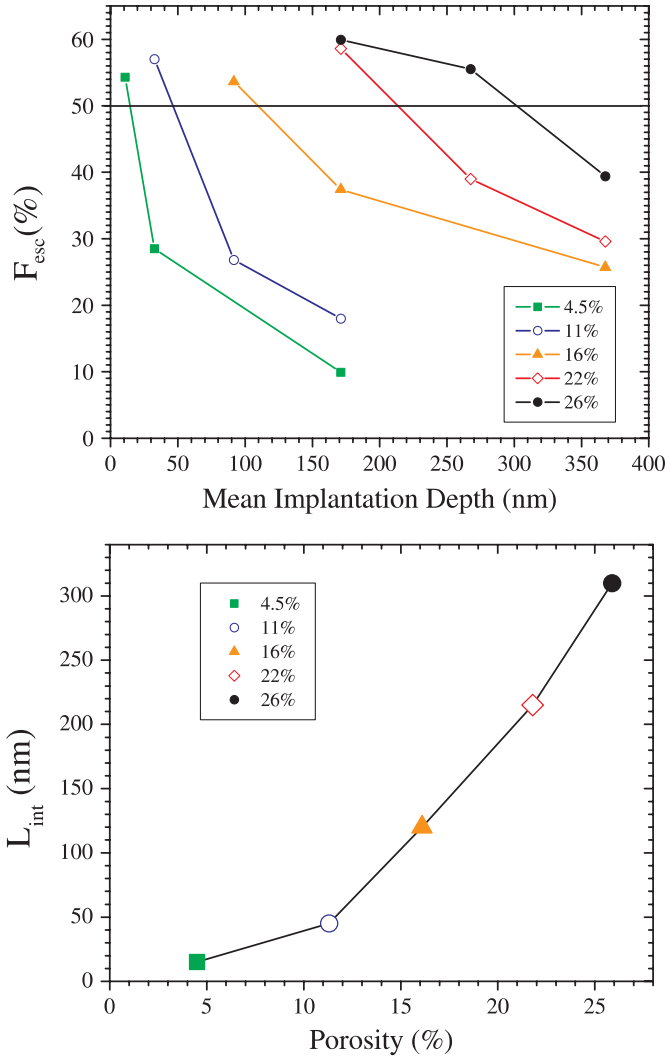

Figure 9 Plot of the Ps escape fraction (F_{esc}) as a function of mean positron implantation depth (*top*) used to calculate the mesopore interconnection length (L_{int}) (*bottom*) for films of increasing porosity. This film is a cyclodextrin-based porogen in a MSSQ matrix.

increases, the deduced value of L_{int} increases rapidly (right plot in Figure 9) because porogen aggregation (not unexpectedly) produces pore clustering that will eventually lead to film percolation (pore interconnection throughout the film). In this particular series of MSSQ-based films, a porogen selected to have a chemically driven propensity for linear aggregation was used (42), and hence the pores present

significant interconnection even at the lowest porosity (which is discussed below in more detail). Less interactive porogens can produce isolated pores ($L_{int} = 0$) for porosities up to 10–20% (for example, see Figure 11 and Figure 13, below). Thus, PALS is providing a very unique view of the film's prepercolation regime, in which finite clustering of the porogen domains, and hence the pores, evolve toward percolation. This provides fundamental information on pore growth and pore shape evolution with film porosity, as we discuss below.

Similar information on the pore interconnection length can be determined from the $3\gamma/2\gamma$ ratio. Figure 10 is a plot of the fraction of total events that annihilate into three photons for films with several different loadings of porogen. The data are then fit to a model Ps atomic diffusion (28) from connected pores into vacuum (the thin line in the bottom panel of Figure 10). The curvature of this fit defines the Ps escape length, which is a measure of pore connectivity. Plots of the interconnection length (determined from the $3\gamma/2\gamma$ technique) versus film porosity

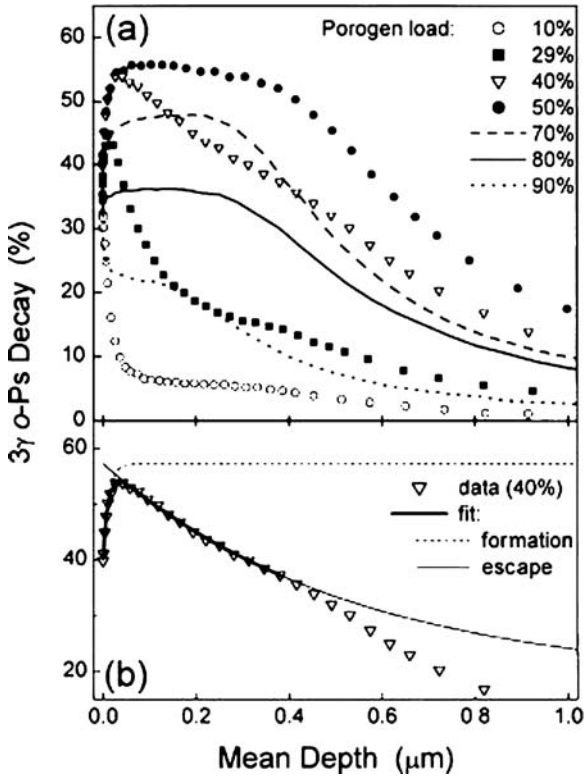

Figure 10 Typical depth-profile of the 3γ fraction for several porogen weight fractions. The lower panel is a fit of the data to a diffusion model to determine L_{int}. Reprinted with permission from Reference 28. Copyright 2005, American Institute of Physics.

18 Jan 2006 10:5 AR ANRV279-MR36-02.tex XMLPublish[SM](2004/02/24) P1: IKH
AR REVIEWS IN ADVANCE10.1146/annurev.matsci.36.111904.135144

are similar to those shown in the right panel of Figure 9. Additionally, the relative fraction (compared to dense films) of 3γ events increases sharply when the pores become interconnected to vacuum, also permitting a unique view of pore clustering (28).

Finally, we note that both the DBS parameters of S and W are also sensitive to the escape of Ps into vacuum (5). This again emphasizes the importance to PAS research of the strong effect of Ps formation and escape into vacuum for all the various PAS spectroscopies. Although DBS would not be the prime technique of choice for probing and measuring pore interconnection length, one can readily deduce the threshold for pore interconnection, as Figure 11 shows.

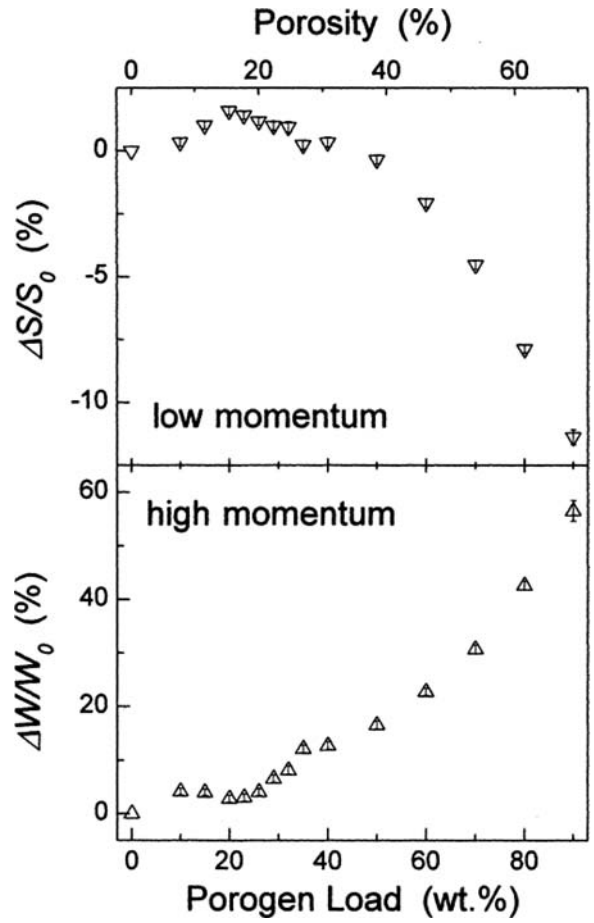

Figure 11 Plot of the change in low-momentum (S) and high-momentum (W) parameters as a function of film porosity. Reprinted with permission from Reference 5. Copyright 2003, American Chemical Society.

18 Jan 2006 10:5 AR ANRV279-MR36-02.tex XMLPublish[SM](2004/02/24) P1: IKH
AR REVIEWS IN ADVANCE10.1146/annurev.matsci.36.111904.135144

DETECTING POROSITY VARIATIONS IN FILM DEPTH In the previous section we indicated how routine depth-profiling can determine the pore interconnection length for a porous film that is homogeneous in depth. What if the film is not homogeneous—i.e., the porosity and/or pore sizes are changing with depth? What if the film is a porous dielectric buried beneath a diffusion barrier or etch stop in a microelectronic device? What if one simply wants to isolate a particular nanoporous layer in a multilayer stack? As indicated in Figure 8, positrons can be implanted at controlled depths to form Ps underneath a surface layer(s) that might normally inhibit absorption in solvent-based porosimetries. Thus, beam-based PAS can be used to study hidden porosity beneath diffusion barriers, dense or capping layers, and multilayer films. Moreover, the diffusion barriers sealing a porous film can be tested for sealing integrity, minimum critical sealing thickness, and thermal stability on any underlying porous film that has interconnected pores (43, 44). PAS is well suited for testing diffusion barriers and advanced sealing strategies, such as plasma surface densification on blanket and patterned low-k dielectric films for microelectronic devices (45). Additionally, depth-profiled PAS investigates inhomogeneities present in as-deposited or processed porous low-k films. For example, plasma densification (pore collapse) can result from exposure to plasmas in microchip processing (45, 46). This type of "integration damage" can severely compromise the dielectric constant reduction by a low-k material (46) and is one of the main impediments in implementing porous, ultralow-k dielectrics in microelectronics.

A good example of the capability of PALS depth-profiling was recently demonstrated in a study of a plasma-enhanced chemical vapor–deposited (PECVD) SiCOH film (47). The depth-dependent PSDs have already been introduced in Figure 6, and they indicate strongly increasing pore size and porosity with film depth. Figure 12 shows a multilayer model for the pore structure of this film that is consistent with the depth-profiled spectra. [Depths in this profile are determined by use of the average density of the film—more (less) dense regions will be proportionately thinner (thicker) than shown.] The top 30 nm of this film appears to be dense (not even microporous), followed by another 30 nm of film that is microporous only. When the film is probed more deeply, 1.5 nm mesopores begin to reveal themselves at depths of 60—170 nm. Even more surprising, at depths greater than 170 nm, another layer at which 3.5-nm-diameter pores dominate the porosity is discovered. In this case, simple PALS depth-profiling alone cannot determine whether the large pores in this buried layer are interconnected, because the upper layers have curtailed the telltale escape of Ps into vacuum. The solution was to combine PALS analysis while progressively etching off the upper layers to effectively move the film surface down to the layer with the 3.5 nm pores. PALS then confirmed (47) the complete escape of Ps into vacuum from these large pores, indicating that they are indeed highly interconnected. This layer of large, interconnected pores is precisely located where Sematech observed trench wall bowing and voids when the researchers etched and Cu-filled 350-nm-deep trenches into this dielectric (48). This integration damage is almost certainly caused by the

18 Jan 2006 10:5 AR ANRV279-MR36-02.tex XMLPublish[SM](2004/02/24) P1: IKH
AR REVIEWS IN ADVANCE10.1146/annurev.matsci.36.111904.135144

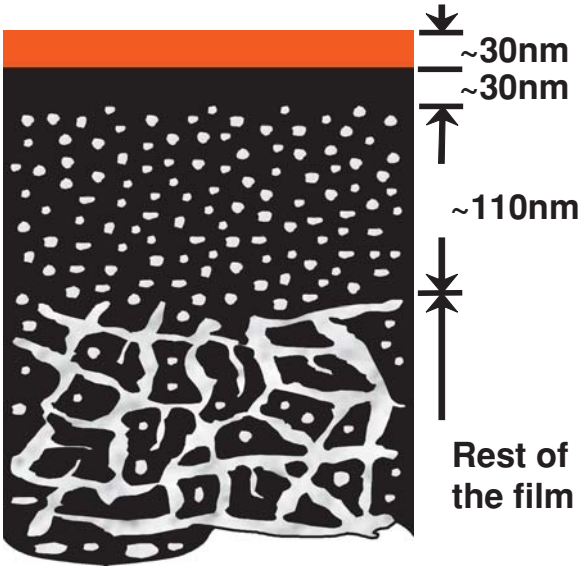

Figure 12 Schematic of the porosity in a PECVD low-k film derived from depth-profiling with PALS.

open pore structure buried deep within this film that manifests itself only when depth-profiling or processing penetrates through the upper sealing layers.

Depth-profiling of thin films using beam-based techniques is a critically important aspect of PAS nanopore characterization. It is fundamental to deducing pore interconnection length and searching for and revealing hidden inhomogeneities in pore morphology. It will prove to be vitally important in studies of integration processing effects on porous dielectric films as well as the correlation of changes in electrical properties with porous structure.

Pore Shape and Growth

Developing an understanding of how pores grow in films with increasing porosity and of the resulting evolution of pore shape is critical for the implementation of controlled pore design. For instance, the chemical role that functional groups of the porogen play in guiding the aggregation of porogen domains in the matrix material is critically important in determining pore size and interconnectivity. Straightforward imaging, if possible, provides only a base understanding of the pores' shape. Traditional permeation techniques in thin films rely on the percolation of the film; i.e., the pores will completely permeate the film. Studies of pore structure and evolution in the prepercolation regime, where there is finite pore clustering, are more difficult. PALS, with its ability to simultaneously characterize the size and interconnection length of the engineered/porogen-induced pores, can

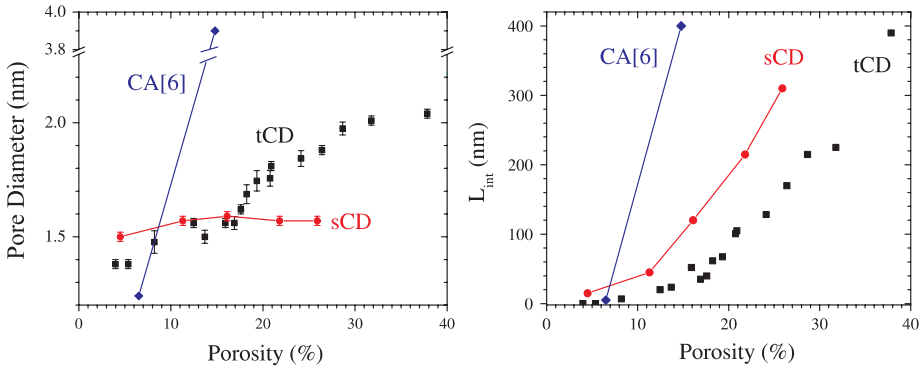

Figure 13 Plots of pore diameter (*left*) and pore interconnection length (*right*) as a function of porosity for MSSQ films made with three different porogens. The growth modes for the porogens are dramatically different.

shed light on the difficult issues of pore shape and its evolution and growth with porosity in the film (24). By studying the evolution of both the pore size and the pore interconnection length, one can begin to deduce the shape of the pores and delineate the relative strength of the porogen-porogen interaction with respect to the porgen-matrix interaction.

In a recent study of the growth of pores in the prepercolation regime, researchers used PALS on films with several cyclodextrin (CD) and calix-arene (CA) porogens with various functional groups in a modified MSSQ host matrix (42). Figure 13 shows results for the pore diameter and L_{int} for films prepared with tCD (CD with methoxyl functional groups), sCD (CD with trimethoxyl-silyl functional groups), and CA. The sCD porogen system produces pores with constant Ps lifetime (hence constant mean-free path) but with interconnection lengths much longer than the pore size for all porosities. To have interconnected pores at the lowest porogen-loading fraction implies that pores are templated from aggregates of at least several porogen molecules. As the loading fraction is increased, the pore diameter remains constant, while the interconnection length continues to increase. Therefore, rather than aggregating in three dimensions, where the pore diameter would be expected to increase, the pores grow linearly. Apparently the trimethoxy-silyl functional groups of sCD are such that they can form Si-O-Si linkages after hydrolysis into silanol groups, and therefore covalently bonded linear chains of sCD molecules are readily formed, producing longer (more interconnected) pores of constant cross section. This growth in the cylindrical (or tubular) length is strikingly clear in Figure 13.

In the tCD system, the methoxyl end-groups are known to have a weaker van der Waals interaction, so the aggregation of the porogen domains is expected to be more three dimensional and random. As seen in Figure 13, at low porosity ($\leq$8%) the pores are isolated ($L_{int} = 0$), with a diameter that is still too large to be consistent

18 Jan 2006 10:5 AR ANRV279-MR36-02.tex XMLPublish[SM](2004/02/24) P1: IKH
AR REVIEWS IN ADVANCE10.1146/annurev.matsci.36.111904.135144

with the size of a single tCD molecule (assuming one-to-one templating into pore volume). Careful analysis resolves that this pore size is consistent with the template of two to three back-to-back porogen molecules, a preferred configuration for such molecules. The pores then gradually increase in pore size and interconnection length as the porosity is increased. This suggests that at low porogen concentration, two to three tCD molecules cluster to form isolated pores and that these two- to three-molecule aggregates become the building blocks for weak, random, three-dimensional aggregation above some threshold porosity, nominally 8% for this system. This trend is consistent with computer simulations of a uniform random population of pores in a matrix, which leads to three-dimensional growth of the pores.

The CA porogen in MSSQ produces very distinct results from those of the CDs in MSSQ in that PALS shows explosive pore growth between 7–15% porosity. The pore diameter jumps drastically from a closed-pore diameter of $\sim$1.2 nm, consistent with the size of the templated molecule, to percolated pores with a diameter of 3.5 nm. The CA molecule, which has a hydrophilic end and a hydrophobic end, acts as a surfactant, which can promote self-assembly and large micelle growth beyond some critical concentration. A more detailed subsequent study using both PALS and ellipsometric porosity (J.-H. Yim, private communication) confirms a critical concentration for micellular growth near 10% porosity and is probing the interesting and precipitous transition in growth mode at this concentration.

These results using an MSSQ host nicely demonstrate the evolution of three different porogen aggregation modes with concentration to create nanoporosity, from isolated pores to interconnected network. PALS results are monitoring the role of functional groups on the CDs and CAs in determining the resulting pore structure evolution (size and interconnection length) versus porosity. These results are a key demonstration of the usefulness of PAS in untangling the fundamental pore structure and its evolution in porosity. Such results provide critical feedback to chemists designing the functional group chemistry that will control the pore structure.

CONCLUSION AND FUTURE IMPROVEMENTS IN PAS CAPABILITIES

Beam-based PAS is a powerful porosimetry technique with broad applicability in characterizing nanoporous films, especially insulators. Pore sizes in the 0.3–30 nm range are derived directly from fitted Ps lifetimes. Plausible distributions of pores can also be determined. Depth-profiling of films with PAS has proven to be an ideal way to measure the interconnection length of mesopores, allows one to search for depth-dependent inhomogeneities in the pore structure in films, and is capable of exploring porosity hidden beneath dense layers, capping layers, and diffusion barriers. PAS has demonstrated its usefulness in the characterization of multilayer films with a complex pore structure and in the investigation of the evolution of

pore shape and structure with porosity. Depth resolution is best near the surface, ~5 nm, and gets progressively longer as deeper implantation yields a broader positron stopping profile. Lateral resolution of several millimeters is typical, but positron microprobes with resolution down to several microns have been made (50, 51). As a research tool for pore characterization in microelectronic materials, PAS, and PALS in particular, offers many attractive porosimetry features with no apparent limitations through the future 22 nm technology node. The positron beam and spectrometer are compact, uncomplicated devices with rather straightforward analysis methodology. Radiation damage to the film is negligible—the technique is nondestructive, with the exception that samples are presently cut to centimeter size from wafers. Cutting wafers and acquiring data for 30 min–1 h are quite acceptable nuisances in a materials research laboratory environment, given the valuable information derived.

At present there are several issues confronting beam-based PAS that limit the scope of its application. These limitations will be considered a preamble to discussing future improvements anticipated in PAS. One unavoidable limitation is the requirement that the target sample must be in vacuum, which would curtail certain liquid- or air-based applications in the life sciences. Another is the requirement that the sample material must form Ps. Most insulating materials readily form Ps, but there are some notable counter examples (e.g., kapton). (We should note that requiring Ps formation is an overstatement because positron annihilation spectroscopies routinely used in metal and semiconductors are applicable, but the application to nanoporous films would be severely hampered.) The present inability of PAS to determine absolute porosity ab initio means that the technique falls one step short of complete pore characterization analysis with a single probe. Some other practical limitations are temporary nuisances and include limitations on the positron beam rate and diameter on sample, which results in spectra requiring 20–60 min to acquire and difficulties in studying patterned microelectronic devices for which patterned fields are at the millimeter scale.

Positron researchers are continuously working to improve PAS techniques to have a broad impact in the development of future nanoporous films. The need for more intense positron beams is universal, and internationally there are many efforts to increase beam rates to 10^8–10^{10} positrons s^{-1}. Delft University of Technology in the Netherlands (31, 52) and FRM in Germany (53) use nuclear reactors to pair-produce positrons. The Japanese facilities at KEK (54) and ETL (55) use linac-generated bremsstrahlung radiation to pair-produce positrons, whereas beams at Washington State University (56) and SHI (57) generate a β^+ source from $C^{12}(d,n)N^{13}$ and $Al^{27}(p,n)Si^{27}$ interactions, respectively, using particle accelerators. At least one company, First Point Scientific, is researching the development of commercial positron beams (58). A new intense positron beam facility is under construction at the North Carolina State University Nuclear Reactor in Raleigh, North Carolina (59). This Delft-inspired positron beam based on pair-production in the intense gamma flux near the reactor core is designed to be the centerpiece of a national center for nanoporosity characterization, including the latest generation

18 Jan 2006 10:5 AR ANRV279-MR36-02.tex XMLPublish[SM](2004/02/24) P1: IKH
AR REVIEWS IN ADVANCE10.1146/annurev.matsci.36.111904.135144

of PALS spectrometers for depth-profiled nanoporosity and nanophase characterization. This National Science Foundation– and Department of Energy–funded facility within the Nuclear Engineering Department at North Carolina State University is intended to allow fast, convenient, and inexpensive access to PALS/PAS analysis and expertise for materials researchers and engineers in both academia and industry. The future access for materials researchers to PAS facilities based around intense positron beams is very promising.

Increased positron beam currents enable beam rate–intensive spectroscopies such as 2D-ACAR and coincidence-DBS to acquire spectra in reasonable periods of time. By contrast, high rates can effectively achieve maximum detector-allowed, dead-time-limited data rates in other spectroscopies, such as PALS and $3\gamma/2\gamma$ ratio, for which spectrum acquisition times will be reduced to under 1 min and perhaps to as little as 10–20 s. Moreover, these detector-limited rates may also be achieved with submillimeter beam spots on target, thus permitting even broader application within, for example, the microelectronics industry.

Future work should improve the understanding of the physics of Ps formation and annihilation in porous insulators. It is somewhat embarrassing that the basic electron-capture process enabling PAS characterization of nanoporous materials is largely understood only at a superficial level—the Ore model and spur model. Porous materials may be the ideal testing ground for investigating the relative contributions and details of these models (38) because systematically varying the film porosity should enhance the Ore capture process at the pore surfaces. Conversely, variation of the target sample's temperature (30) should preferentially enhance the spur model electron-positron capture parameters, allowing additional differentiation of the two processes. The importance of understanding Ps formation goes beyond curiosity in the fundamental physics. Ps formation is one root cause why PAS cannot presently deduce absolute film porosity. Moreover, on a related issue, not knowing the fundamentals of Ps formation leads to confusion over chemistry-related modifications to a film as opposed to changes in porous morphology. We have frequently observed process-induced modifications to the surface of a film by, for example, plasma exposures of different chemical compositions. Yet one cannot be sure if the observed reduction in Ps formation in the film's porogen-induced pores is related to reduced porosity/pore collapse and/or chemical modifications from the plasma that reduce Ps formation. The untangling of these competing effects would be facilitated by a better understanding of how a film's chemical and material properties influence Ps formation. In a similar fashion, it is important to continue to improve the pore size calibration and search for the inevitable material specificity (at some level of accuracy) that should be inputted into the extended Tao-Eldrup models. Pore shape dependence of the Ps lifetime should also receive further attention (60). Deducing a PSD is not exact or unique, and efforts are certainly continuing to hone this capability.

The use of PAS in nanotechnology applications has surged significantly in the past 5–10 years, especially within industry. Although much of this attention stems from extensive efforts by microelectronic firms and their suppliers to replace silica

as the interlayer dielectric in microchips with low-k alternatives, it should also be acknowledged that thin, amorphous, insulating films with nanometer-scale pores are inherently challenging to traditional porosimetry techniques. Innovation in pore metrology has attempted to accompany innovation in nanotechnology, and PAS has emerged as one of only three to four viable pore characterization techniques available for submicron amorphous films. To this end PAS may well find fruitful applications in other fields involving any material for which the voids or pores influence the material's properties or performance. Selectable porous membranes (61) such as those found in fuel cells (62) may benefit from pore characterization by PAS, as may porous hydrogen storage devices. Porous interconnects in photovoltaic devices that produce high surface area for charge collection may benefit from PAS analysis. PAS is certainly involved in understanding the role of voids and open-volume defects in porous film diffusion barriers (63), in understanding environmental damage in photoresists (64), and recently in probing barrier technology on organic LEDs (65). With positron beam intensity improvements already underway both in this country and abroad, the materials researcher should find unprecedented access to PAS techniques to meet the growing demand for standardized structural characterization at the nanometer scale.

ACKNOWLEDGMENTS

We would like to thank Albert Yee of the California Institute for Telecommunications and Information Technology, Robert Miller and Qinghuang Lin of IBM, Todd Ryan of AMD, Do Yoon of Seoul National University, Richard Carter of LSI Logic, Jin-heong Yim of Kongju National University, Carol Mohler of Dow Chemical, and Ayman Hawari of North Carolina State University for their collaborations. The continuing support of the Low-k Dielectric Program of Sematech International is gratefully acknowledged. We thank other members of the Michigan Positron Group, Mark Skalsey, William Frieze, and Ming Liu for dedicated support.

The *Annual Review of Materials Research* is online at http://matsci.annualreviews.org

LITERATURE CITED

1. Polarz S, Smarsly B. 2002. Nanoporous materials. *J. Nanosci. Nanotechnol.* 2:581–612
2. Schultz PJ, Lynn KG. 1988. Interaction of positron beams with surfaces, thin films, and interfaces. *Rev. Mod. Phys.* 60:701
3. Pethrick RA. 1997. Positron annihilation—a probe for nanoscale voids and free volume? *Prog. Polym. Sci.* 22:1–47
4. Gidley DW, Lynn KG, Petkov MP, Weber MH, Sun JN, Yee AF. 2001. Depth-profiled positron lifetime spectroscopy of thin insulation films. In *New Directions in Antimatter Chemistry and Physics*, ed. CM Surko, FA Gianturco, pp. 151–71. Dordrecht, The Netherlands: Kluwer Acad. Publ.
5. Petkov MP, Wang CL, Weber MH, Lynn KG, Rodbell KP. 2003. Positron

annihilation techniques suited for porosity characterization of thin films. *J. Phys. Chem. B* 107:2725–34
6. Ito K, Kobayashi Y. 2005. Variable-energy positron annihilation as highly sensitive nanoporosimetry for porous thin films. *Acta Phys. Pol. A* 107:717–23
7. Charlton M, Humberston JW. 2001. *Positron Physics*. Cambridge, U.K: Cambridge Univ. Press. 454 pp.
8. Mogensen OE. 1982. Positronium formation in condensed matter and high-density gases. In *Positron Annihilation*, ed. PG Coleman, SC Sharma, LM Diana, pp. 763–72. Amsterdam: North Holland
9. Dauwe C, Van Waeyenberge B, De Baerdemaeker J. 2005. Experimental verification of the blob model and delayed formation of Ps. *Acta Phys. Pol. A* 107:623–28
10. Byakov VM, Stepanov SV. 1996. Common features in the formation of Ps, Mu, radiolytic hydrogen and solvated electrons in aqueous solutions. *J. Radioanal. Nucl. Chem.* 210:371–405
11. Vallery RS, Zitzewitz PW, Gidley DW. 2003. Resolution of the orthopositronium-lifetime puzzle. *Phys. Rev. Lett.* 90: 203402
12. Schrader DM, Jean YC. 1988. *Positron and positronium chemistry*. Amsterdam: Elsevier. 395 pp.
13. Eldrup M, Lightbody D, Sherwood JN. 1981. The temperature-dependence of positron lifetimes in solid pivalic acid. *Chem. Phys.* 63:51–58
14. Tao SJ. 1972. Positronium annihilation in molecular substances. *J. Chem. Phys.* 56:5499–510
15. Dull TL, Frieze WE, Gidley DW, Sun JN, Yee AF. 2001. Determination of pore size in mesoporous thin films from the annihilation lifetime of positronium. *J. Phys. Chem. B* 105:4657–62
16. Jasinska B, Dawidowicz AL, Goworek T, Wawryszczuk J. 2003. Pore size determination by positron annihilation lifetime spectroscopy. *Opt. Appl.* 33:7–12
17. Coleman PG. 2000. *Positron Beams and Their Applications*. Singapore: World Sci. Publ. Co. 322 pp.
18. Siegel RW. 1980. Positron-Annihilation Spectroscopy. *Annu. Rev. Mater. Sci.* 10:393–425
19. Weber MH, Hunt AW, Golovchenko JA, Lynn KG. 1999. Energy-resolved positron annihilation in flight in solid targets. *Phys. Rev. Lett.* 83:4658–61
20. Stoll H, Bandzuch P, Siegle A. 2001. Positron-age-momentum correlation. In *Positron Annihilation—Icpa-12*, ed. W Triftshäuser, G Kögel, P. Sperr, pp. 547–51. Uetikon-Zürich, Switzerland: Trans Tech Publ., Inc.
21. Mondal NN, Hamatsu R, Hirose T, Iijima H, Irako M, et al. 1999. Construction of a time-of-flight measurement system to study the low energy positronium production. *Appl. Surf. Sci.* 149:269–75
22. Yu RS, Ohdaira T, Suzuki R, Ito K, Hirata K, et al. 2003. Positronium time-of-flight measurements of porous low-k films. *Appl. Phys. Lett.* 83:4966–68
23. Ito K, Nakanishi H, Ujihira Y. 1999. Extension of the equation for the annihilation lifetime of ortho-positronium at a cavity larger than 1 nm in radius. *J. Phys. Chem. B* 103:4555–58
24. Wang CL, Weber MH, Lynn KG, Rodbell KP. 2002. Nanometer-scale pores in low-k dielectric films probed by positron annihilation lifetime spectroscopy. *Appl. Phys. Lett.* 81:4413–15
25. Gidley DW, Frieze WE, Dull TL, Yee AF, Ryan ET, Ho HM. 1999. Positronium annihilation in mesoporous thin films. *Phys. Rev. B* 60:R5157–60
26. Brusa RS, Spagolla M, Karwasz GP, Zecca A, Ottaviani G, et al. 2004. Porosity in low dielectric constant SiOCH films depth profiled by positron annihilation spectroscopy. *J. Appl. Phys.* 95:2348–54
27. Xu J, Moxom J, Yang S, Suzuki R, Ohdaira T. 2002. Dependence of porosity in methylsilsesquioxane thin films on molecular weight of sacrificial triblock copolymer. *Chem. Phys. Lett.* 364:309–13

28. Petkov MP, Weber MH, Lynn KG, Rodbell KP. 2001. Porosity characterization by beam-based three-photon positron annihilation spectroscopy. *Appl. Phys. Lett.* 79:3884–86
29. Weber MH, Lynn KG. 2003. Positron Porosimetry. In *Principles and Applications of Positron & Positronium Chemistry*, ed. YC Jean, PE Mellon, DM Schrader, pp. 163–202. Singapore: World Sci. Publ. Co.
30. Fischer CG, Weber MH, Wang CL, McNeil SP, Lynn KG. 2005. Positronium in low temperature mesoporous films. *Phys. Rev. B* 71:180102
31. Schut H, van Veen A, Falub CV, de Roode J, Labohm F. 2001. Performance of an intense nuclear-reactor based positron beam. In *Positron Annihilation—Icpa-12*, ed. W Triftshäuser, G Kögel, P. Sperr, pp. 430–32. Uetikon-Zürich, Switzerland: Trans Tech Publ., Inc.
32. Kirkegaa P, Eldrup M. 1974. Positronfit extended—new version of a program for analyzing positron lifetime spectra. *Comput. Phys. Commun.* 7:401–9
33. Kansy J. 1996. Microcomputer program for analysis of positron annihilation lifetime spectra. *Nucl. Instrum. Meth. Phys. Res. A* 374:235–44
34. Shukla A, Peter M, Hoffmann L. 1993. Analysis of positron lifetime spectra using quantified maximum-entropy and a general linear filter. *Nucl. Instrum. Meth. Phys. Res. A* 335:310–17
35. Gregory RB, Zhu YK. 1990. Analysis of positron-annihilation lifetime data by numerical Laplace inversion with the program CONTIN. *Nucl. Instrum. Meth. Phys. Res. A* 290:172–82
36. Gidley DW, Frieze WE, Dull TL, Sun J, Yee AF, et al. 2000. Determination of pore-size distribution in low-dielectric thin films. *Appl. Phys. Lett.* 76:1282–84
37. Wang YY, Nakanishi H, Jean YC, Sandreczki TC. 1990. Positron-annihilation in amine-cured epoxy polymers—pressure-dependence. *J. Polym. Sci. B* 28:1431–41
38. Kajcsos Z, Liszkay L, Duplatre G, Varga L, Lohonyai L, et al. 2005. Positronium trapping in porous solids: means and limitations for structural studies. *Acta Phys. Pol. A* 107:729–37
39. Sun JN, Gidley DW, Hu YF, Frieze WE, Yang S. 2002. Characterizing porosity in nanoporous thin films using positron annihilation lifetime spectroscopy. *Mater. Res. Soc. Symp. Proc*. 726:Q10.5
40. Vallery RS, Peng H-G, Frieze WE, Gidley DW, Moore DL, Carter RJ. 2005. Depth-profiling pore morphology in nanoporous thin films using positronium lifetime annihilation spectroscopy. *Mater. Res. Soc. Symp. Proc.* 863:B1.6
41. Mogilnikov KP, Baklanov MR, Shamiryan D, Petkov MP. 2004. A discussion of the practical importance of positron annihilation lifetime spectroscopy percolation threshold in evaluation of porous low-K dielectrics. *Jpn. J. Appl. Phys. 1* 43:247–48
42. Peng H-G, Vallery RS, Frieze WE, Liu M, Gidley DW, et al. 2005. Deducing pore structure and growth in nanoporous thin films. *Appl. Phys. Lett.* 87:161903
43. Sun JN, Hu YF, Frieze WE, Chen W, Gidley DW. 2003. How pore size and surface roughness affect diffusion barrier continuity on porous low-k films. *J. Electrochem. Soc.* 150: F97–101
44. Sun JN, Gidley DW, Dull TL, Frieze WE, Yee AF, et al. 2001. Probing diffusion barrier integrity on porous silica low-k thin films using positron annihilation lifetime spectroscopy. *J. Appl. Phys.* 89:5138–44
45. Sun JN, Gidley DW, Hu Y, Frieze WE, Ryan ET. 2002. Depth-profiling plasma-induced densification of porous low-k thin films using positronium annihilation lifetime spectroscopy. *Appl. Phys. Lett.* 81:1447–49
46. Ryan ET, Freeman M, Svedberg L, Lee JJ, Guenther T, et al. 2003. A study of atomic layer deposition and reactive plasma compatibility with mesoporous organosilicate glass films. *Mater. Res. Soc. Symp. Proc.* 766:E10.8
47. Peng HG, Frieze WE, Vallery RS, Gidley

DW, Moore DL, Carter RJ. 2005. Revealing hidden pore structure in nanoporous thin films using positronium annihilation lifetime spectroscopy. *Appl. Phys. Lett.* 86:121904

48. Liu Y, Knorr A, Wu W-L, Gidley DW, Kastenmeier B. 2005. Pore structure and integration performance of a porous CVD ultra low k dielectric. *Mater. Res. Soc. Symp. Proc.* 863:B3.11
49. Deleted in proof
50. Triftshäuser W. 2004. Positron microprobes. In *Positron Annihilation—Icpa-13, Proceedings*, ed. T Hyodo, Y Kobayashi, Y Nagashima, H Saito, pp. 452–56. Uetikon-Zürich, Switzerland: Trans Tech Publ., Inc.
51. David A, Kogel G, Sperr P, Triftshauser W. 2001. Lifetime measurements with a scanning positron microscope. *Phys. Rev. Lett.* 87(6):067402
52. van Veen A, Labohm F, Schut H, deRoode J, Heijenga T, Mijnarends PE. 1997. Testing of a nuclear-reactor-based positron beam. *Appl. Surf. Sci.* 116:39–44
53. Hugenschmidt C, Kogel G, Repper R, Schreckenbach K, Sperr P, et al. 2002. Intense positron source at the Munich research reactor FRM-II. *Appl. Phys. A* 74:S295–97
54. Kurihara T, Yagishita A, Enomoto A, Kobayashi H, Shidara T, et al. 2000. Intense positron beam at KEK. *Nucl. Instrum. Meth. Phys. Res. B* 171:164–71
55. Suzuki R, Ohdaira T, Mikado T, Ohgaki H, Chiwaki M, Yamazaki T. 1997. Control and measurement system for positron experiments at the ETL linac facility. *Appl. Surf. Sci.* 116:187–91
56. Hunt AW, Pilant L, Cassidy DB, Tjossem R, Shurtliff M, et al. 2002. The development of the intense positron beam at Washington State University. *Appl. Surf. Sci.* 194:296–300
57. Hirose M, Nakajyo T. 1999. The SHI slow positron beam facility with a compact cyclotron. *Appl. Surf. Sci.* 149:24–29
58. First Point Scientific, Inc. http://www.firstpsi.com
59. Hathaway AG. 2005. *Design and testing of a prototype slow positron beam at the NC State University PULSTAR reactor*. Masters thesis. North Carol.State Univ. 90 pp.
60. Consolati G. 2002. Positronium trapping in small voids: influence of their shape on positron annihilation results. *J. Chem. Phys.* 117:7279–83
61. Merkel TC, Freeman BD, Spontak RJ, He Z, Pinnau I, et al. 2002. Ultrapermeable, reverse-selective nanocomposite membranes. *Science* 296:519–22
62. Rajendran RG. 2005. Polymer electrolyte membrane technology for fuel cells. *MRS Bull.* 30:587–90
63. Xu J, Mills AP, Case C. 2005. Measuring the continuity of diffusion barriers on porous films using γ-ray energy spectra of escaping positronium. *Appl. Phys. Lett.* 87:054105
64. Dean KR, Meute J, Rich G, Turnquest K, Patel S, et al. 2004. Effect of airborne molecular contamination on 157 nm photoresists. *Abstr. Papers ACS* 228:U427–U Pt. 2
65. Zambov L, Weidner K, Shamamian V, Camilletti R, Pernisz U, et al. 2005. Advanced CVD silicon carbide barrier technology for protection from detrimental gases. *48th Annual Technical Conference Proceedings of the Society of Vacuum Coaters.* In press